**Advances in Materials Research**, *Vol. 13, No. 6 (2024) 507-525*
https://doi.org/10.12989/amr.2024.13.6.507


# Investigation on polyvinyl butyral interlayered and ultrasonic vibration-assisted friction stir welded AA7075-T651 joints

Vaibhav S. Gaikwad[1a] and Satish Chinchanikar*[2]

[1]*Department of Mechanical Engineering, Vishwakarma Institute of Information Technology, Pune-411048, India*
[2]*Department of Mechanical Engineering, Vishwakarma Institute of Technology, Pune-41103, India*

(*Received November 30, 2022, Revised October 16, 2024, Accepted October 21, 2024*)

**Abstract.** In this study, the performance of polyvinyl butyral interlayered friction stir welded (PVBFSWed) and ultrasonic vibration-assisted friction stir welded (UVaFSWed) AA7075-T651 joints are investigated, considering the effect of tool rotation and welding speed. The joints' tensile strength, microhardness, microstructure, and fracture behavior are evaluated. The UVaFSWed joints showed better performance compared to the PVBFSWed joints. The highest tensile strength of 322.8 MPa and microhardness of 157 Hv in weld nugget is observed for the UVaFSWed joint at a tool rotation of 2000 rpm and welding speed of 40 mm/min. However, the lowest surface roughness of 7.98 μm was observed for the UVaFSWed joint at a tool rotation of 1400 rpm and welding speed of 40 mm/min. Comparatively lower tensile strength and microhardness were observed for the PVBFSWed joints compared to UVaFSWed joints. The fracture for the UVaFSWed and PVBFSWed joints mainly occurred in the heat-affected zone during the tensile test. The scanning electron microscopy (SEM) images show the more uniform, equiaxed grain distribution in the UVaFSWed joint.

**Keywords:** AA7075; friction stir welding; interlayer; polyvinyl butyral; ultrasonic vibrations

## 1. Introduction

Nowadays, every industrial sector is looking for new cost-effective paths to reduce the weight of the products, raise the speed of their vehicles, airplanes, and missiles or reduce greenhouse gases produced during manufacturing. Therefore, research is continuing innovative joining techniques to realize material compounds and to get closer to these several goals. AA7075 aluminum alloy, with its low density and better mechanical properties, finds wide applications in the aerospace, defense, military, and automotive sectors. It is a precipitation-hardenable alloy with magnesium, zinc, and copper as the main alloying elements. Friction stir welding (FSW) is preferred to join aluminum alloys due to liquation cracking and solidification observed with fusion welding (Cetkin *et al*. 2019).

The FSW process is preferred to join difficult-to-weld similar and dissimilar aluminum alloys. Being a solid-state joining process, FSW leads to lower distortion and residual stress. FSW produces

*Corresponding author, Professor, Ph.D., E-mail: satish.chinchanikar@vit.edu
[a] Ph.D., E-mail: vaibhav.219p0007@viit.ac.in


http://www.techno-press.org/?journal=amr&subpage=5 ISSN: 2234-0912 (Print), 2234-179X (Online)

better joints compared with other fusion welding techniques. In the FSW process, a specially designed non-consumable rotating tool is inserted into the abutting edges of the workpieces to be joined and is moved along the line of the interface of two plates. Consequently, the softened material near the tool is transported from the advancing side to the retreating side to form a joint (Chinchanikar and Gaikwad 2021).

In the FSW, a high downward force and spindle torque are required to generate high heat. The heat generated softens the material to ensure adequate plastic flow adjacent to the tool. It leads to the condition of a larger volume of welding equipment and a higher welding load (Arora *et al*. 2011).

The FSW tool pin profile is subjected to higher stress during welding that causes rapid tool wear leading to premature failure. Moreover, the tool wear causes poor weld quality resulting in higher production costs. Also, the higher welding load in the FSW limits the welding speed. These difficulties can be addressed using different secondary energy sources during FSW. A group of researchers applied ultrasonic vibrations during the FSW. Ultrasonic vibration-assisted friction stir welding (UVaFSW) assists in softening the material without substantial heating (Shi *et al*. 2015, Yao *et al*. 2012, Siddiq and Sayed 2011).

Liu and Wu (2013) found that ultrasonic vibration-assisted FSW enhanced the joint mechanical properties, the quality of the weld, and the heat input at the localized area. Xu *et al*. (2016) observed that ultrasonic vibration-assisted welding brazing produced a joint with a finer grain size that enhanced corrosion resistance and ultimate tensile strength (UTS). Liu *et al*. (2015), while investigating UVaFSW of AA1060 aluminum alloy, found that ultrasonic energy enhanced the flow velocity, the volume of deformed material, and the strain rate.

A group of researchers observed enhancement in the mechanical properties, material flow, weld appearance, and decrement in weld porosity and tool wear using ultrasonic vibration-assisted FSW of aluminum alloys (Shakil *et al*. 2014, Lei *et al*. 2018, Kumar *et al*. 2017, Wu *et al*. 2017, Zhong *et al*. 2017). The ultrasonic vibrations during FSW increased the fatigue life by lowering the stress concentration at the bonding region (Wu *et al*. 2017). Zhong *et al*. (2017) observed improved material flow, a reduction in the axial force, and tool torque requirement due to the assistance of ultrasonic vibrations to FSW.

Liu and Wu (2016), while joining AA2024-T4 aluminum alloy, observed higher microhardness at the weld nugget (WN) and tensile strength compared to the FSW joint. Gao *et al*. (2016), while joining AA6061-T6 aluminum alloy using UVaFSW, found a higher strain component that assisted in the refinement of the grain. A group of researchers observed that the assistance of the ultrasonic vibrations to FSW helped in breaking the intermetallic compounds (IMC) and improving the UTS of the joint (Liu *et al*. 2018, Meng *et al*. 2018).

The ultrasonic vibrations to FSW provided higher deformation characteristics, a finer grain structure, and continuous material flow in the weld bead (Padhy *et al*. 2016a, Liu and Wu. 2015). Gao *et al*. (2017) observed higher material flow, lower flow stress, and ductile fracture while joining AA2024-T3 aluminum alloy using UVaFSW against joining with FSW. Subgrain formation at weld nugget, improved bonding, breakage of the intermetallic compound into smaller particles, and the ductile mode of failure can be achieved by imposing ultrasonic vibrations to FSW (Padhy *et al*. 2016b, Meng *et al*. 2017, Lv *et al*. 2017).

Shi *et al*. (2016) simulated UVaFSW by superimposing the ultrasonic vibrations on the workpiece. Their study observed enhanced material flow, strain rate, and plastic deformation. The ultrasonic vibrations generate more heat in the WN, which improves the mechanical properties and lowers the corrosion resistance, intermetallic compound, and requirement for torque and axial force (Kumar *et al*. 2016, Thomä *et al*. 2018, Lv *et al*. 2017). Hu *et al*. (2021) observed higher UTS of

355-361 MPa for the UVaFSWed high-strength 2219 aluminum alloy joint at the welding speed range of 300-600 mm/min and at a constant tool rotation of 800 rpm. Zhang *et al*. (2020) found around a 9% reduction in axial force and an 8.8% increase in elongation while joining 7N01-T4 aluminum alloy using UVaFSW against FSW.

A group of researchers observed an earlier start of the nucleation, many lower-size grains, and better material flow and strain rate in UVaFSW against the conventional FSW (Yang *et al*. 2020, Wu *et al*. 2021, Zhao *et al*. 2020). The ultrasonic vibrations encouraged the aggregation, motion, and annihilation of dislocations in weld nuggets and improved the mechanical properties by around 10-25% (Chowdhury *et al*. 2021, Zhao *et al*. 2022, Muhammad *et al*. 2021, Su *et al*. 2022).

A group of researchers also attempted FSW with the application of interlayer between the two joining plates to obtain better mechanical properties and fatigue strength for the welded joint. Mokabberi *et al*. (2018) investigated the effect of zinc, copper, and brass interlayers during the FSW. Their study revealed that the joint efficiency improved from 60 to 90% by using the brass interlayer. The copper and zinc interlayers marginally improved joint efficiency. The microstructural observations show that the brass interlayer was distributed and shattered in the WN. Khorrami *et al*. (2014) investigated the FSW of AA1050 aluminum alloy by using SiC nano-particles as interlayers. The interlayer during the FSW reduced the grain size in the WN and improved the microhardness in WN, TMAZ, and HAZ. Moreover, the SiC nanoparticles improved the UTS and microhardness compared to the conventional FSW.

A group of researchers found improvement in the shear tensile strength of the FSW joint with zinc interlayer (Kuang *et al*. 2015, Boucherit *et al*. 2017). Lenin *et al*. (2016), while FSW of AA7020 aluminum alloy, revealed that the joint UTS, grain size, and microhardness vary with the thickness of the zinc interlayer. The zinc interlayer thickness of 10 μm produced better UTS, fined grains, and microhardness. However, very few attempts are observed on FSW considering the effect of interlayer on the mechanical properties of the of aluminum alloys welded joint.

The literature reviewed shows that the UVaFSW and interlayered FSW improved the mechanical properties and material flow. However, limited studies are observed on friction stir welded (FSWed) of AA7075-T651 joints considering the effect of ultrasonic vibrations and an interlayer. With this view, the present work evaluates the performance of polyvinyl butyral interlayered friction stir welded (PVBFSWed) and ultrasonic vibration-assisted friction stir welded (UVaFSWed) AA7075 joints. The experiments were performed with conical threaded pin-type tools varying the tool rotation and welding speed. The joints' tensile strength, microhardness, microstructure, and fracture behavior are evaluated. The material flow and joint fracture surfaces are investigated with SEM images. The results are compared with the available literature on FSW of AA7075 joints produced using conical and conical threaded tool pin profiles.

## 2. Experimental details

In this study, the AA7075-T651 square butt FSW joints are produced using a polyvinyl butyral (PVB) layer as an interlayer between the two joining plates and with ultrasonic vibrations, respectively. The experimental setup is shown in Figs. 1 and 2, respectively. Experiments were performed with welding speeds of 20, 28, and 40 mm/min and tool rotations of 1000, 1400, and 2000 rpm. Experiments were performed on a universal milling machine using the conical threaded tool. Two plates to be welded were initially squared and made free from any burr and oil to ensure a clean and smooth surface. Experiments were performed under dry conditions without heating the plates. The absence of heating prevents any potential distortion or weakening of the plates.

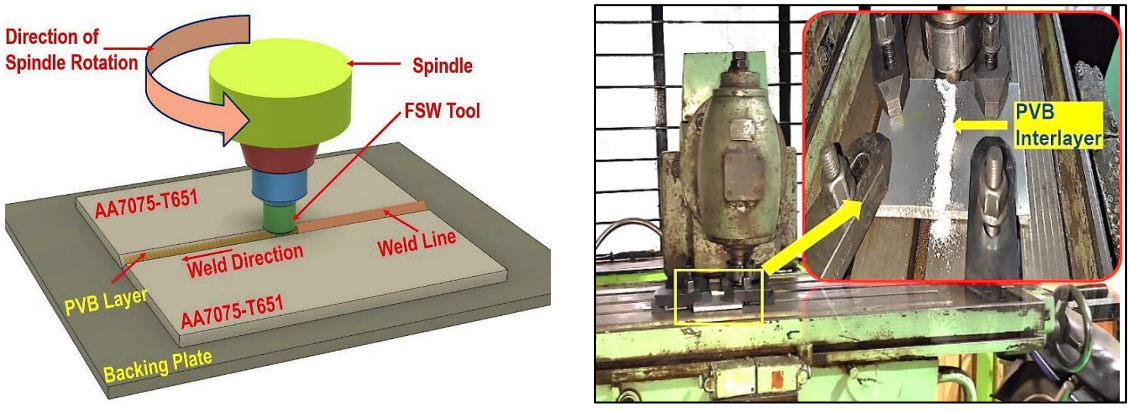


(a) Schematic view (b) Experimental setup

Fig. 1 Application of interlayer during FSW process

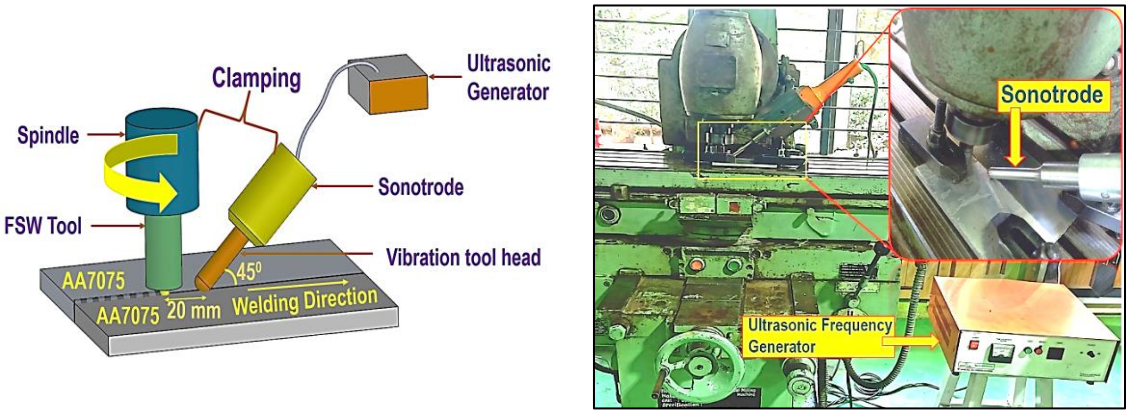


(a) Schematic view (b) Experimental setup

Fig. 2 UVaFSW process

The faying edges of the plates are machined into the smooth surface and cleaned with acetone. Then, the PVB interlayer is placed between the plates of AA7075-T651, as depicted in Fig. 1. The PVB has a melting point of 120°C and chemical composition as polyvinyl butyral 81%, polyvinyl alcohol ~18-23 %, and polyvinyl acetate < 1%.

The ultrasonic vibrations generated using an ultrasonic transducer propagate through an amplitude transformer to magnify the amplitude and concentrate the energy at the weld line of two plates. This energy is transmitted to the localized workpieces near and ahead of the FSW tool by a sonotrode. The ultrasonic vibrations at a frequency of 20 kHz and output power of 1.2 kW is applied during the welding process. The amplitude of the vibration tool head is 24 μm when no load exerts on it. The vibration direction is 45° tilted from the workpiece plane. The distance from the ultrasonic action point to the axis of the FSW tool is 20 mm. A schematic view and experimental set up of UVaFSW process are shown in Fig. 2.

A tool with translatory and rotary motions provides thermo-mechanical action along the weld direction. The tool material is H13-type tool steel and has a flat shoulder with a conical threaded pin, as depicted in Fig. 3 (Gaikwad and Chinchanikar 2021a, b, 2022a). The tool shoulder transfers

Table 1 The chemical composition (% weight) of H13 FSW tool (Gaikwad and Chinchanikar 2021a, b)

| Elements | Cr | Mo | Si | V | C | Ni | Cu | Mn | P | S |
|---|---|---|---|---|---|---|---|---|---|---|
| % | 4.75 | 1.10 | 0.80 | 0.80 | 0.32 | 0.3 | 0.25 | 0.2 | 0.03 | 0.03 |

Table 2 Chemical composition (% weight) of AA7075-T651 alloy (Gaikwad and Chinchanikar 2021a, b)

| Elements | Si | Fe | Cu | Mn | Mg | Zn | Ni | Pb | Sn | Ti | Cr | Al |
|---|---|---|---|---|---|---|---|---|---|---|---|---|
| % | 0.06 | 0.2 | 1.64 | 0.006 | 2.33 | 5.28 | 0.01 | 0.01 | <0.005 | 0.02 | 0.19 | 90.2 |

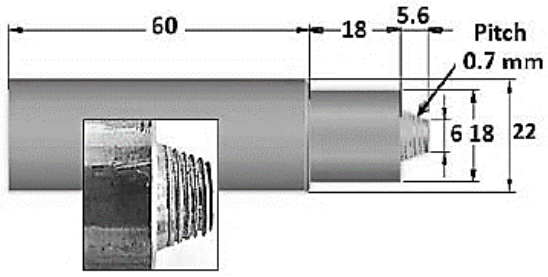


Fig. 3 Conical threaded pin type tool (All dimensions are in mm)

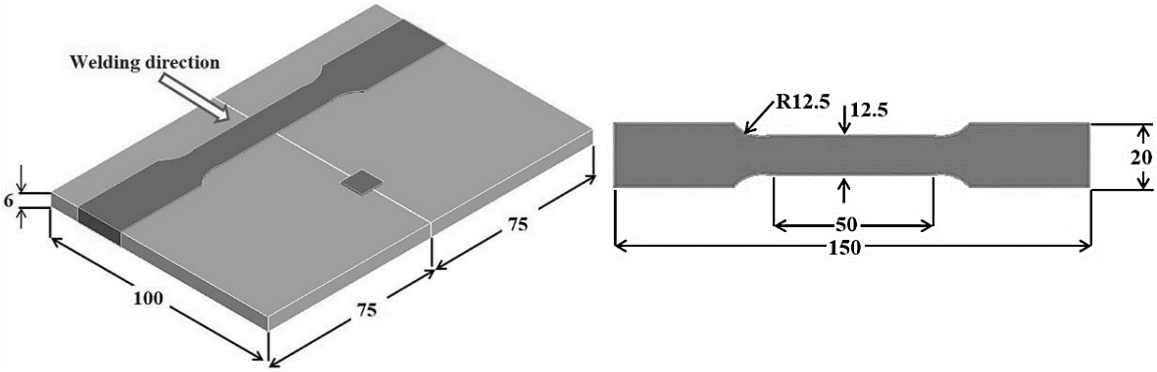


(a) Plate showing position for extraction of test specimens

(b) Tensile test specimen

Fig. 4 Test specimens (dimensions are in mm)

the axial load on the work surface. The pin transfers plasticized material along the joint length. The chemical compositions of the tool and workpiece materials are depicted in Tables 1 and 2, respectively. The values shown are averages of measurements taken at three repeated chemical composition tests, aiming to ensure accuracy, minimize variations, and minimize outliers or anomalies, and then used for data analysis. The microstructure of the joints at different welding zones and the material flow in the weld nugget are studied using SEM images of the sample shown as the dark cube in Fig. 4 (a). The mechanical properties of the joint, such as the ultimate tensile strength (UTS), microhardness at weld nugget (WN), thermo-mechanically affected heat zone (TMAZ), Heat affected zone (HAZ), and base metal (BM), and surface roughness (Ra) are investigated considering the influence of process parameters.

Table 3 Experimental matrix with mechanical properties for PVBFSWed AA7075-T651 joints

| Run | Tool rotation (rpm) | Welding speed (mm/min) | UTS (MPa) | Joint efficiency (%) | Microhardness (Hv) | | | Surface roughness (μm) |
|---|---|---|---|---|---|---|---|---|
| | | | | | WN | TMAZ | HAZ | |
| A1 | 1000 | 20 | 143.70 | 26.13 | 113 | 105 | 94 | 17.15 |
| A2 | 1000 | 28 | 139.17 | 25.31 | 131 | 119 | 102 | 13.42 |
| A3 | 1000 | 40 | 105.95 | 19.26 | 145 | 125 | 110 | 13.5 |
| A4 | 1400 | 20 | 174.49 | 31.73 | 133 | 118 | 98.8 | 15.29 |
| A5 | 1400 | 28 | 142.57 | 25.92 | 131 | 112 | 103 | 17.37 |
| A6 | 1400 | 40 | 132.60 | 24.11 | 127 | 115 | 105 | 11.33 |
| A7 | 2000 | 20 | 152.77 | 27.78 | 121 | 110 | 103 | 15.85 |
| A8 | 2000 | 28 | 92.89 | 16.89 | 151 | 130 | 110 | 13.46 |
| A9 | 2000 | 40 | 197.59 | 35.93 | 156 | 133 | 98.8 | 24.37 |

The FSWed joint transverse UTS, efficiency, and percentage elongation were evaluated for all the joints obtained at different process parameters. A tensile test is performed on a universal testing machine referring to the ASTME8M standard. Figs. 4(a) and (b) show the AA7075 aluminum alloy plate showing the position for extraction of the test specimen and extracted tensile test specimen, respectively.

The microhardness at WN, TMAZ, HAZ, and BM was measured using Vicker's microhardness tester as per the ISO6507 standard using the diamond indenter (136$^{o}$) with a load of 100 grams and a dwell time of 20 seconds. The average surface roughness, measured at the start, middle, and end of the weld, was obtained.

The joint microstructure at different welding zones and the material flow in the WN are observed using a Field Emission Scanning Electron Microscope (FESEM) at different magnifications. The samples are cut in the transverse direction to the weld line by wire electric discharge machining.

## 3. Results and discussion

This section discusses the performance of polyvinyl butyral interlayered friction stir welded (PVBFSWed) and ultrasonic vibration-assisted friction stir welded (UVaFSWed) AA7075-T651 joints. Tensile strength, microhardness, fracture behavior, and microstructure of welded joints are evaluated considering the effect of welding speed and tool rotation. The UTS of the base material obtained after the tensile test is 550 MPa.

The experimental matrix with the mechanical properties for the FSW using the application of PVB as interlayer (Run A1 to A9) and using the UVaFSW (Run B1 to B9) are represented in Tables 3 and 4, respectively.

### *3.1 Mechanical properties of PVBFSWed and UVaFSWed AA7075-T651 joints*

Stress-strain curves for AA7075-T651 PVBFSWed joints (Run A1 to A9) and UVaFSWed joints (Run B1 to B9) are as shown in Figs. 5 (a) and (b), respectively. The variation of UTS for AA7075-T651 PVBFSWed joints (Run A1 to A9) and UVaFSWed joints (Run B1 to B9) are as shown in Figs. 6(a) and (b), respectively.

Table 4 Experimental matrix with mechanical properties for UVaFSWed AA7075-T651 joints

| Run | Tool rotation (rpm) | Welding speed (mm/min) | UTS (MPa) | Joint efficiency (%) | Microhardness (Hv) | | | Surface roughness (μm) |
|---|---|---|---|---|---|---|---|---|
| | | | | | WN | TMAZ | HAZ | |
| B1 | 1000 | 20 | 278.01 | 50.55 | 145 | 126 | 117 | 7.98 |
| B2 | 1000 | 28 | 264.55 | 48.10 | 148 | 132 | 121 | 12.06 |
| B3 | 1000 | 40 | 272.59 | 49.56 | 150 | 141 | 131 | 11.4 |
| B4 | 1400 | 20 | 241.76 | 43.96 | 152 | 135 | 125 | 9.29 |
| B5 | 1400 | 28 | 251.45 | 45.72 | 153 | 141 | 119 | 13.53 |
| B6 | 1400 | 40 | 268.74 | 48.86 | 144 | 136 | 124 | 11.35 |
| B7 | 2000 | 20 | 309.78 | 56.32 | 153 | 141 | 132 | 8.52 |
| B8 | 2000 | 28 | 312.48 | 56.82 | 158 | 142 | 135 | 13.46 |
| B9 | 2000 | 40 | 322.80 | 58.69 | 157 | 146 | 132 | 18.05 |

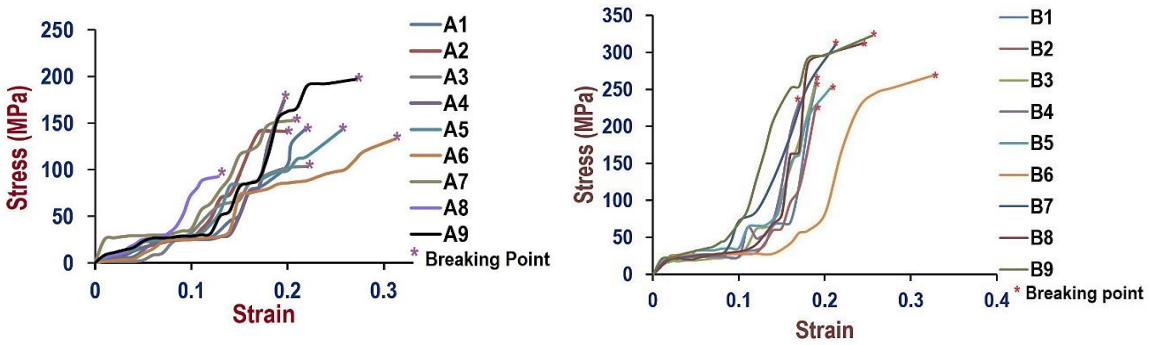


(a) PVBFSWed AA7075-T651 joint (b) UVaFSWed AA7075-T651 joint

Fig. 5 Stress-strain curves for AA7075-T651 joints

The maximum UTS of 197.59 MPa is observed for AA7075-T651 PVBFSWed joint at tool rotation of 2000 rpm and welding speed of 40 mm/min (Run A9). The comparatively higher UTS is obtained for AA7075-T651 PVBFSWed joint against the conventional FSW of AA7075 (Gaikwad and Chinchanikar 2021a, 2021b, 2022a). The improved performance of the PVBFSWed joint could be attributed to the increased bonding between the plates due to the PVB interlayer. PVBFSWed joint also showed comparatively higher fracture energy and strength against the conventional FSWed joint. The PVB, with a low melting point compared to the AA7075, melts faster and travels into the weld pool. The dispersion of PVB particles in the WN gives higher strength to the joint.

The findings of this study are in better agreement with the researchers' work with different interlayers during FSW of similar and dissimilar aluminum alloys (Mokabberi *et al*. 2018, Khorrami *et al*. 2014, Kuang *et al*. 2015, Boucherit *et al*. 2017, Lenin *et al*. 2016). Kumar *et al*. (2019) found enhanced mechanical properties, microstructure, and corrosion resistance for the joints produced with the interlayer. These joints also showed lower intermetallic compounds and residual stress. Khajeh *et al*. (2022) observed better strength and ductility for the FSWed AA2024 aluminum alloy and copper joints with the Zn interlayer.

The maximum UTS of 322.8 MPa (Run B9) is observed for the UVaFSWed AA7075-T651 joint at tool rotation of 2000 rpm and welding speed of 40 mm/min. The UTS for UVaFSWed joints is

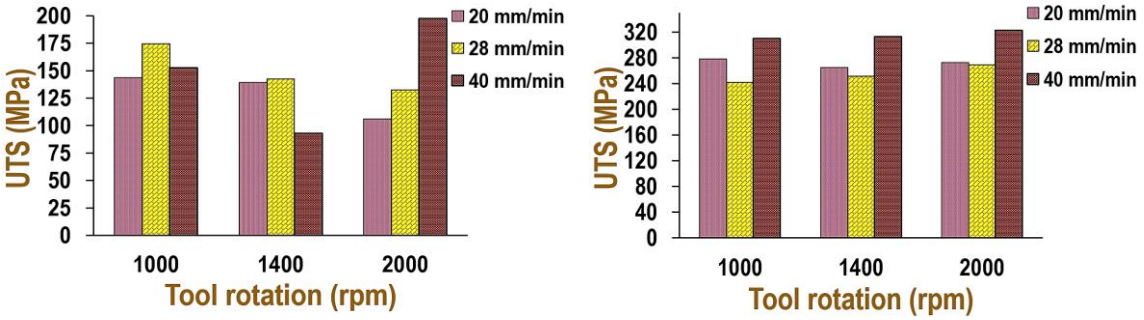


(a) PVBFSWed joint (b) UVaFSWed joint

Fig. 6 Variation of UTS for AA7075-T651 joints

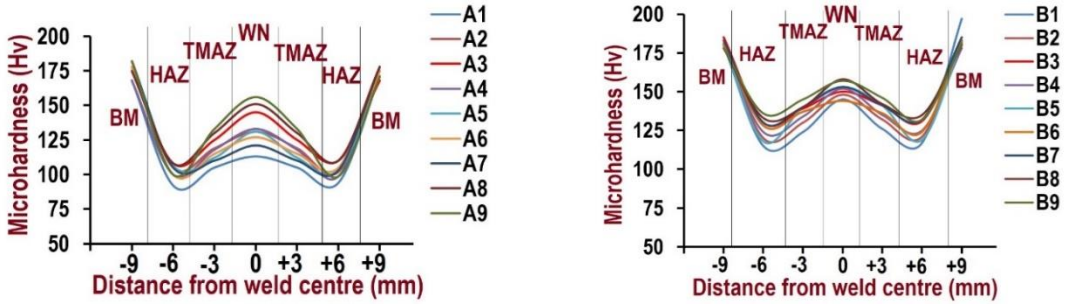


(a) PVBFSWed joint (b) UVaFSWed joint

Fig. 7 Variation of microhardness for AA7075-T651 joints

higher than the FSWed (Gaikwad and Chinchanikar 2021a, 2021b, 2022a) and PVBFSWed interlayered AA7075 joints. The higher mechanical properties with the UVaFSWed joints could be attributed to an increased strain rate leading to higher plastic deformation and better material flow around the tool pin due to the ultrasonic vibrations. A group of researchers observed better mechanical properties for the UVaFSWed for similar-dissimilar aluminum alloy joints (Gao *et al*. 2016, Padhy *et al*. 2016, Kumar *et al*. 2019).

From Figs. 6(a) and (b), the higher UTS are obtained at a tool rotation of 2000 rpm and a welding speed of 40 mm/min. However, no significant improvement in UTS can be seen with an increase in tool speed and welding speed for UVaFSWed joints. On the other hand, for PVBFSWed joints, UTS can be seen as initially decreasing with the tool speed and welding speed and then increasing at the tool rotation of

2000 rpm and welding speed of 40 mm. This could be attributed to the fact that the higher tool rotation increases the frictional heat between the tool shoulder and surface of the workpiece. The increased frictional heat softens the material and enhances its movement to the weld pool, resulting in uniform mixing of the material. This study suggests a scope for further studies on the investigation of mechanical properties of UVaFSWed joints varying with the ultrasonic frequencies.

The microhardness of PVBFSWed and UVaFSWed AA7075-T651 joints were measured at several points from the weld center on both sides of the joint, as shown in Figs. 7 (a) and (b), respectively. The severe extrusion and higher plastic deformation cause variations in the grain size and the microhardness in the welded region. The microhardness of joints produced using PVB as an

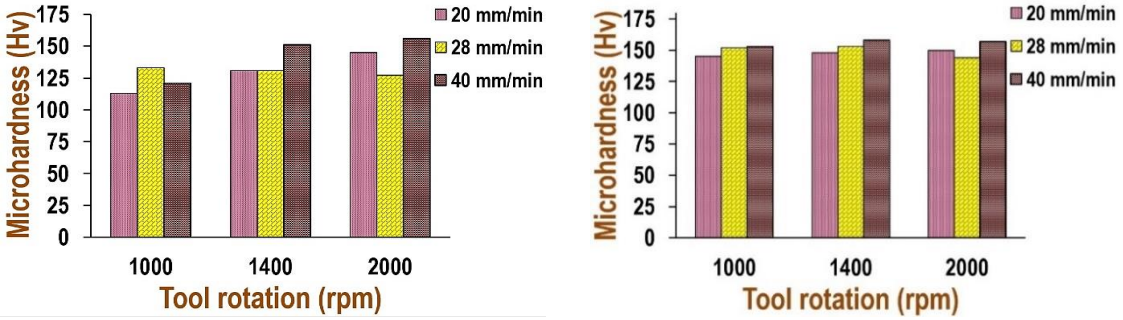


(a) PVBFSWed joint (b) UVaFSWed joint

Fig. 8 Microhardness at WN for AA7075-T651 joints

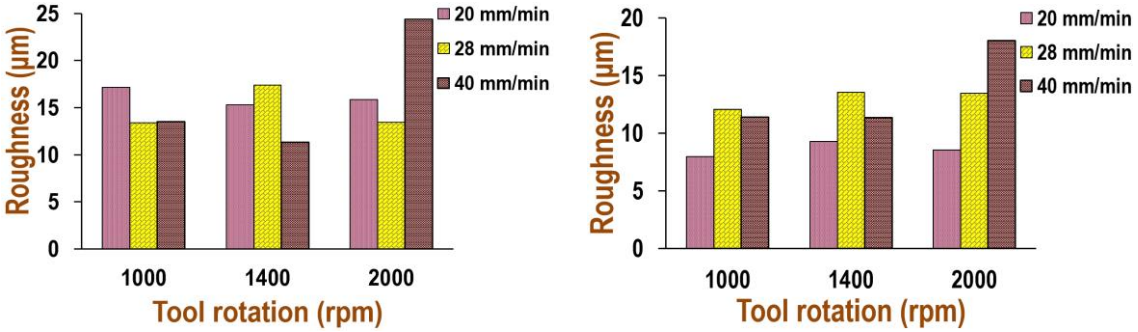


(a) PVBFSWed joint (b) UVaFSWed joint

Fig. 9 Surface roughness for AA7075-T651 joints

interlayer and UVaFSW showed variation in the welding zone, mostly following the distribution of a letter 'W' shape, and found maximum at the WN and minimum at the HAZ. A higher microhardness was obtained for PVBFSWed, and UVaFSWed joints compared FSWed joints (Liu and Wu 2016, Gao *et al*. 2017, Gaikwad and Chinchanikar 2021a, 2022b).

The microhardness at WN varying with process parameters for the PVBFSWed and UVaFSWed joints are shown in Figs. 8(a) and(b), respectively. Higher microhardness at WN, TMAZ, and HAZ is obtained for UVaFswed joints at higher tool rotation against PVBFSWed and FSWed joints (Gaikwad and Chinchanikar 2021a). The ultrasonic vibrations with higher tool rotation enhanced the heat generation, plastic deformation and eliminated tunnel defects resulting in higher microhardness at the weld bead (Gao *et al*. 2017, Gaikwad and Chinchanikar 2022b). However, the PVBFSWed joints showed better mechanical properties against the FSWed joints (Gaikwad and Chinchanikar 2021a, 2022b). It could be attributed to the better bonding between the PVB interlayered joining plates. The UVaFSWed joints sustained higher tensile loads, which could be attributed to higher heat input due to application of ultrasonic frequency at the weld bead. Moreover, ultrasonic vibration to the weld bead assisted in dynamic recrystallization and improved the material movement towards the weld bead. Further, the assistance of ultrasonic vibrations also reduced weld defects/flaws in the WN and its interfaces with TMAZ compared with the conventional FSWed joints (Gaikwad and Chinchanikar 2021a, 2022b). The analysis of the joints at different weld zones is discussed with the SEM images in section 3.2.

The joint quality was assessed by obtaining the surface roughness. Figs. 9(a) and (b) show the

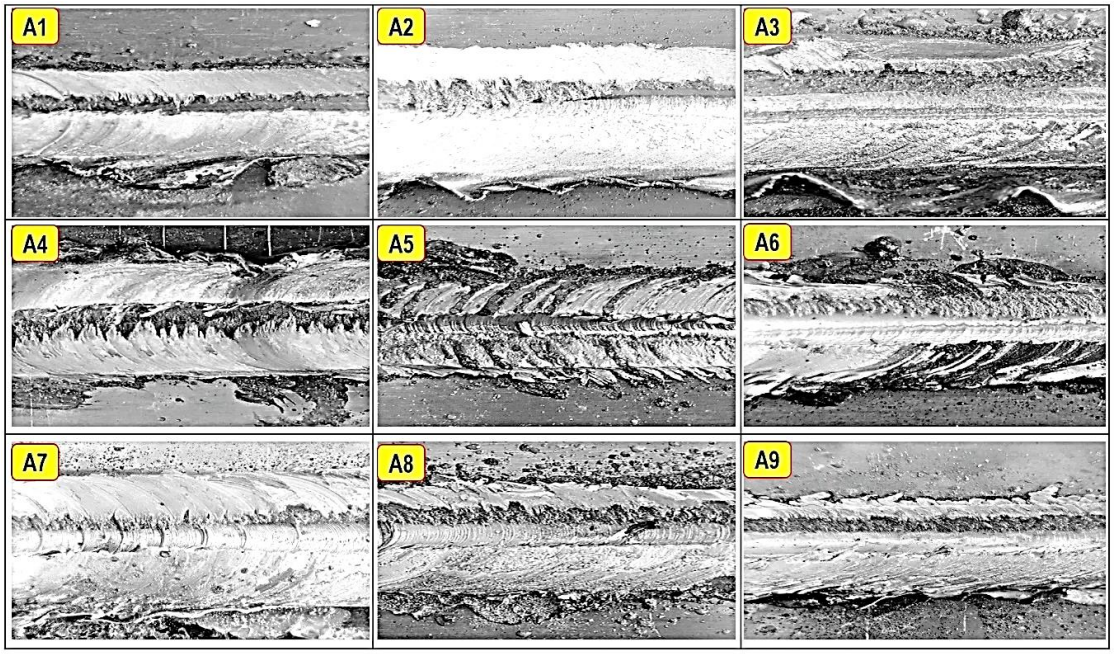


Fig. 10 Weld top surface of PVBFSWed AA7075-T651 joints

surface roughness for the PVBFSWed and UVaFSWed AA7075 joints, respectively, varying with process parameters. Average surface roughness of 11-26 µm and 7-18 µm can be seen for the PVBFSWed and UVaFSWed AA7075 joints, respectively. However, lower surface roughness was observed for the conventional FSWed joints compared to the PVBFSWed (Gaikwad and Chinchanikar 2021a). The appearance of fined PVB powder particles on the weld bead leads to higher surface roughness. The lowest surface roughness of 7.98 µm for UVaFSWed joints can be seen at welding speed and tool rotational speed of 20 mm/min and 1000 rpm (run B1). It could be due to the uniform material mix in the weld bead because of ultrasonic vibrations. A group of researchers also observed lower surface roughness while UVaFSW of similar and dissimilar aluminum alloys (Muhammad and Wu 2019, Zhang *et al*. 2020).

Figs. 10 and 11 show the top surface appearance for the PVBFSWed and UVaFSWed AA7075 joints, respectively. From the figures, the formations of the onion ring can be seen that indicate the uniform and proper mixing of the material in the weld bead that eliminated the voids and tunnel defects. The joints with filled material in the weld bead and the smoother top surface can be seen for UVaFSWed joints compared to PVBFSWed joints.

The lower surface roughness for the UVaFSWed joints could be attributed to UAFSW's high-frequency vibrations that improve the material's plastic flow around the tool. The smoother material flow leads to a more uniform consolidation at the weld surface, reducing surface imperfections and enhancing surface quality. UVaFSW effectively reduces defects like surface grooves, voids, and incomplete fusion, which are prevalent in conventional FSW. The improved material movement fills gaps and inconsistencies in the weld seam, resulting in a smoother surface. Ultrasonic vibrations reduce tool resistance, thereby reducing the total forces required for the welding process. By lessening tool-induced surface markings and imperfections, this reduction in friction enables a smoother interaction between the tool and the material, directly improving surface roughness.

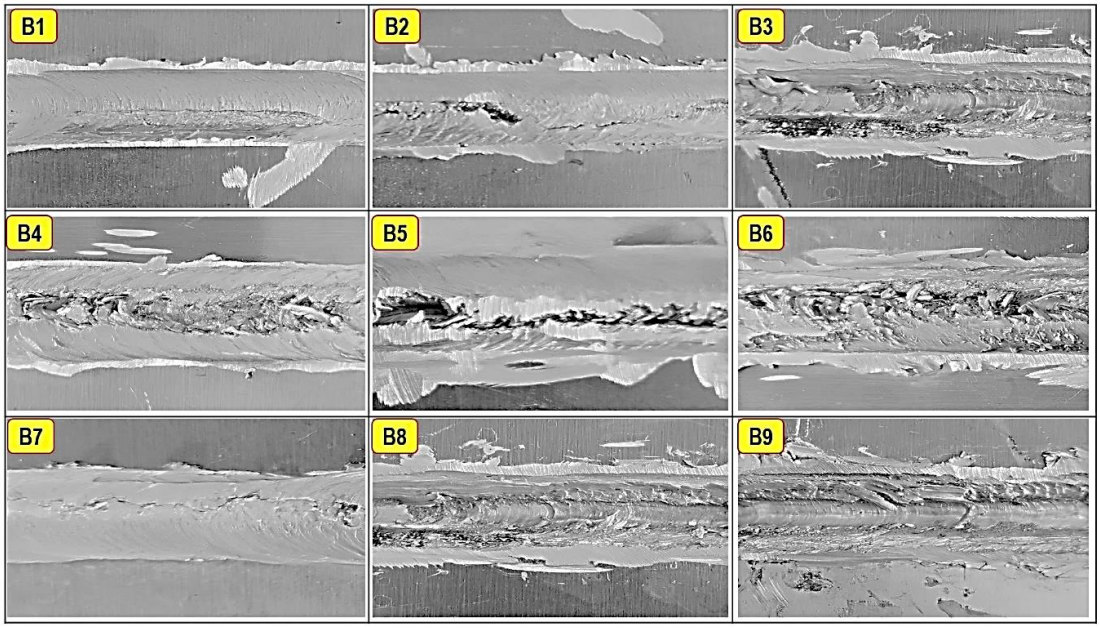


Fig. 11 Weld top surface of UVaFSWed AA7075-T651 joints

Throughout the welding process, the reduced tool wear and better material contact aid in maintaining a constant surface finish. A tool with reduced wear generates a more even surface without sacrificing quality. Ultrasonic vibrations near the welding surface promote a finer grain structure, leading to better mechanical qualities and a smoother surface. By removing the broad, uneven grain boundaries that can result in rough surfaces, the finer and more uniform grains help to reduce surface roughness. In general, friction stir welding with ultrasonic vibration assistance improves surface quality over PVBFSWed AA7075-T651 joints by increasing material flow, decreasing tool-induced defects, and better managing heat input.

### *3.2 Microstructure of PVBFSWed and UVaFSWed AA7075-T651 joints*

Figs. 12(a)-(f) show the SEM images of WN, TMAZ, and HAZ of the PVBFSWed and UVaFSWed joints obtained at run A9 and B9, respectively. The homogeneous grain distribution at WN, fine dispersion of PVB particles at the WN, and absence of tunnel defects can be seen in Fig. 12(a). These attributes resulted in a higher UTS for the PVBFSWed joint compared to the conventional FSWed joint [49]. The grain size of ~ 865 nm-7 µm can be seen at the WN. However, fine, equiaxed, and uniformly distributed grains having size ~649 nm-5 µm at the WN of the UVaFSWed joint can be seen in Fig. 12(b). The UVaFSW improves the grain size at WN and material flow inside the weld bead compared to the conventional FSW.

Fig. 12(c) depicts the SEM image of TMAZ of the PVBFSWed joint. Homogeneous mixing of material with dispersed PVB can be seen. The coarser distributed grains than those at WN differentiates this weld region. This weld region is adjacent to WN. The grains having coarser sizes of ~ 6-8 µm can be seen at TMAZ. It could be due to less heat distribution from WN to TMAZ. Fig. 12(d) depict SEM image of TMAZ of a UVaFSWed joint. Equiaxed and homogeneous distribution of grains with sizes varying in the range of ~3-7 µm can be seen.

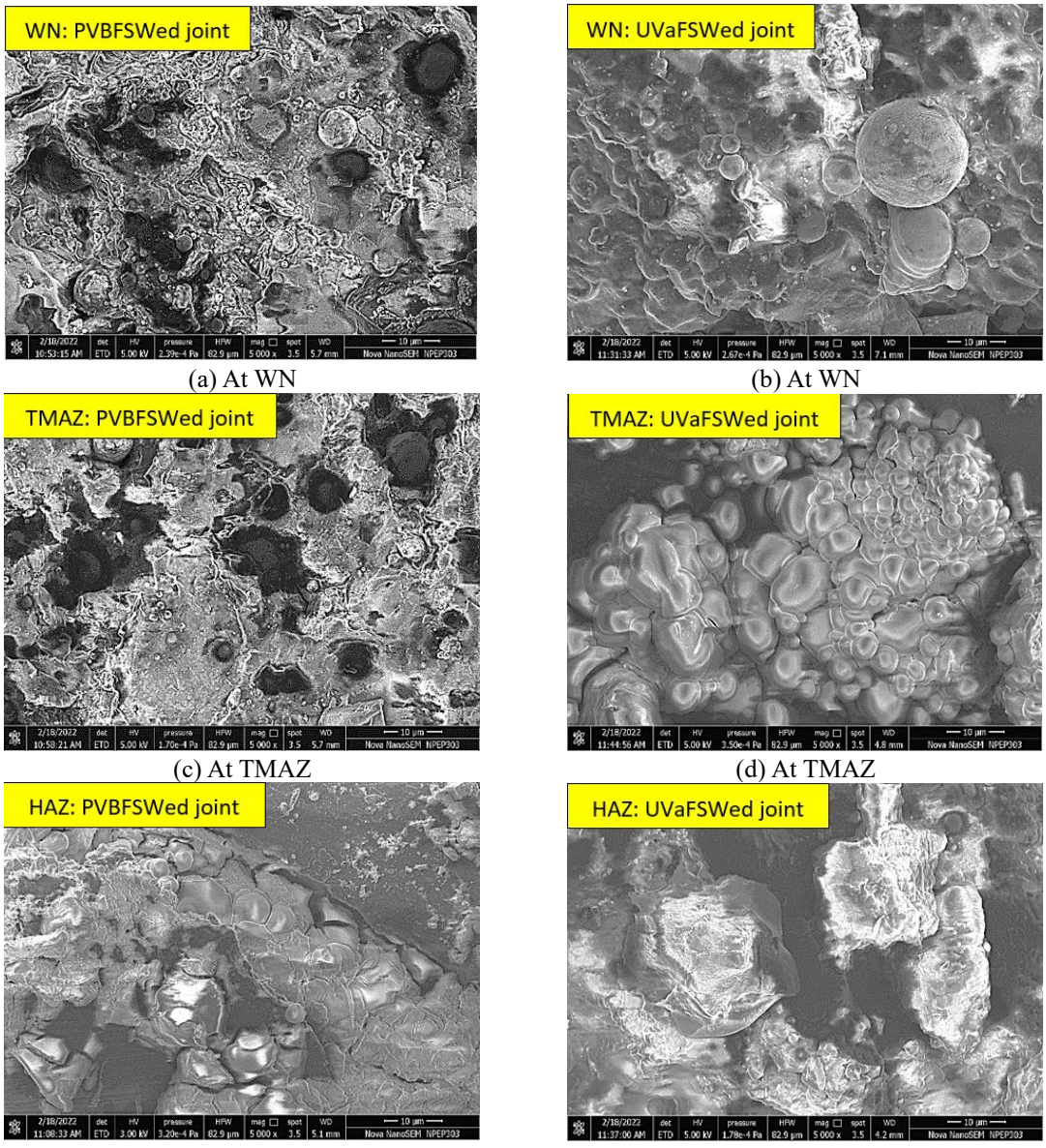


(a) At WN (b) At WN

(c) At TMAZ (d) At TMAZ

(e) At HAZ (f) At HAZ

Fig. 12 SEM images of the PVBFSWed and UVaFSWed joints

Fig. 12(e) depicts a coarser and elongated grain distribution with grain sizes of ~ 9-12 µm than those observed at WN and TMAZ. This weld zone is between the TMAZ and the base metal (BM) and is designated as HAZ. The coarser grain size at HAZ shows a comparatively low-temperature region than TMAZ and WN. The reduction in microhardness with an increase in grain size can be seen from the WN to HAZ. The highest microhardness observed at WN is 156 Hv, followed by 133 Hv at TMAZ and 98.8 Hv at HAZ. The SEM images confirm the uniform diffusion and presence of PVB particles at the interface of AA7075 aluminum plates. A group of researchers observed finer

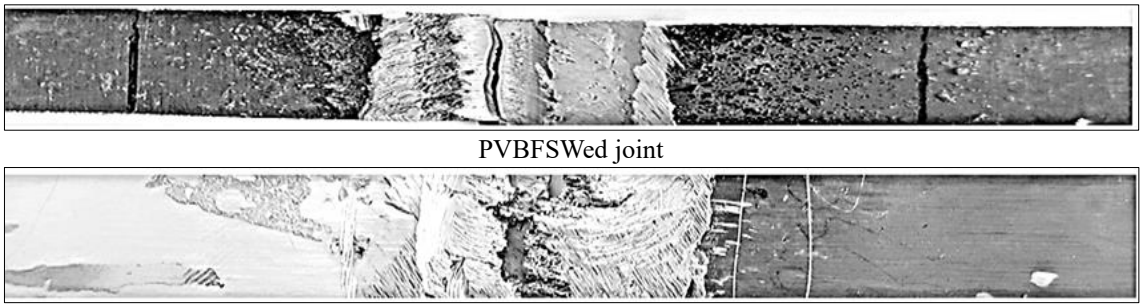

PVBFSWed joint

UVaFSWed joint

Fig. 13 Fracture behavior of AA7075-T651 joints

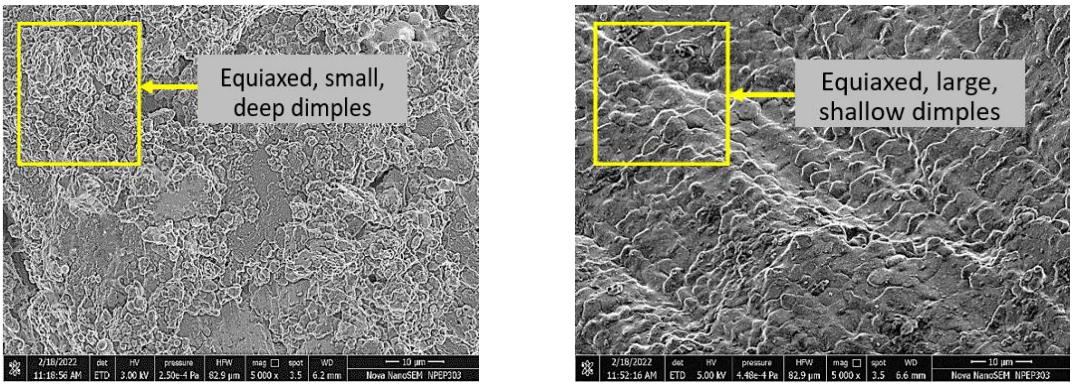


(a) PVBFSWed joint (b) UVaFSWed joint

Fig. 14 SEM images of fractured surface of AA7075-T651 joints

grains at the WN than at TMAZ and HAZ and the appropriate diffusion of interlayer on the interface of FSWed joints (Liu *et al*. 2022, Kumar and Wu 2021). Fig. 12(f) depicts SEM image of HAZ of a UVaFSWed joint which shows elongated grains having the size of ~7-12 µm.

SEM images show that the UVaFSW improves the grain size at WN and material flow inside the weld bead compared to the PVBFSW and conventional FSW. Fine, equiaxed, and uniformly distributed grains at the WN can be seen for the UVaFSWed joint. The higher mechanical properties obtained for the UVaFSWed joints can be confirmed from SEM images showing higher plastic deformation, dynamic recrystallization, and better material flow toward the weld bead.

### *3.3 Fracture behavior of PVBFSWed and UVaFSWed AA7075-T651 joints*

Figs. 13 (a)-(b) shows the fractured specimens of AA7075-T651 PVBFSWed and UVaFSWed joints obtained at run A9 and B9, respectively. They are fetched side by side after the tensile test. This study observes that all the test specimens are fractured in the HAZ, and ductile behavior during the fracture. SEM images of fractured surface specimens of the PVBFSWed joint and UVaFSWed joint obtained at run A9 and B9 are depicted in Figs. 14 (a) and (b), respectively.

Deep and small dimples in the PVBFSWed specimen represent the lower plastic deformation. However, large, and shallow dimples in the UVaFSWed test specimen show higher plastic

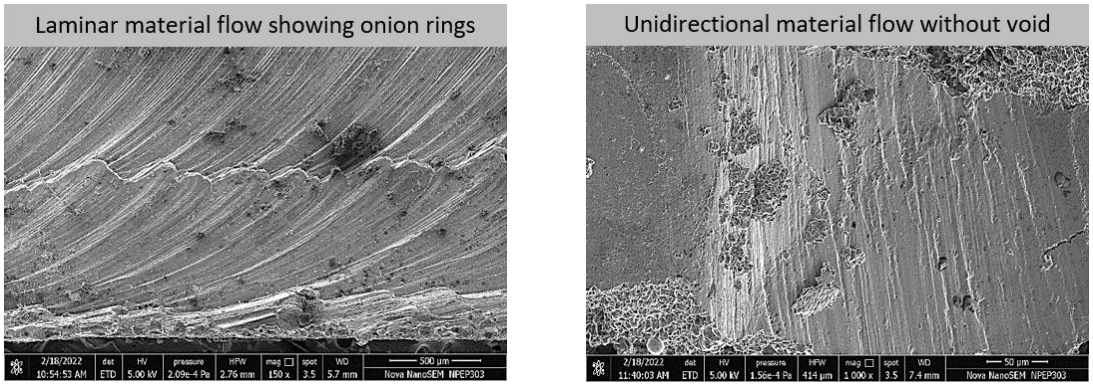


(a) PVBFSWed joint (b) UVaFSWed joint

Fig. 15 Material flow of AA7075-T651 joints

deformation. The dimple sizes impact the sustainability of plastic deformation during tensile testing. On the other hand, the dimples observed for the PVBFSWed specimen are larger and equiaxed than that of the fractured conventional FSWed test specimen. Hence, the UTS, microhardness in different weld regions, and surface roughness are superior for PVBFSWed and UVaFSWed joints compared to the conventional FSWed joint (Gaikwad and Chinchanikar 2022b).

The diverse fracture behaviors observed for the PVBFSWed and UVaFSWed joints can be correlated with the generated heat during the process. More heat is generated in UVaFSW due to the dual effect of ultrasonic frequency and frictional heat produced by the tool shoulder. Higher the heat generation, higher the plastic deformation and material flow resulting in the higher values of UTS and microhardness. A group of researchers also correlated the large and equiaxed dimples observed on the fracture surface with the higher values of UTS and microhardness of FSWed joints (Liu *et al*. 2018, Gao *et al*. 2017, Ji *et al*. 2017).

### *3.4 Material flow of PVBFSWed and UVaFSWed AA7075-T651 joints*

The quality of the weld depends on the flow of pasty material beneath the tool during FSW. Figs. 15 (a) and (b) show the material flow at the WN during FSW with PVB as an interlayer (at run A9) and UVaFSW (at run B9), respectively. The laminar material flow is observed at runs A9 and B9.

The microstructure observed PVBFSWed and UVaFSWed AA7075-T651 joints obtained at run A9 and B9, respectively, is free from defect and porosity compared to the conventional FSWed joint (Gaikwad and Chinchanikar 2022b). However, the formation of onion rings is observed in the case of the PVBFSWed joint. It indicates the proper intermixing of the material at WN. The mixing of the material improves the mechanical properties of the joints. On the other hand, uniform material flow is observed in the WN of the UVaFSWed joint. The tunnel defect and micro void are eliminated due to the ultrasonic vibrations. The ultrasonic vibrations improve the fusion between the material, resulting in higher mechanical properties compared to conventional FSWed and PVBFSWed joints.

Compared to traditional FSW and PVBFSW, UAFSW considerably affected the evolution of microstructural features, particularly grain boundary movement and dynamic recrystallization. Ultrasonic vibrations boosted material energy during welding, enhancing atomic mobility and accelerating grain boundary movement compared to conventional FSW. Ultrasonic vibrations enhanced dynamic recrystallization by increasing dislocation density and subgrain density,

facilitating faster grain nucleation and more efficient recrystallization compared to conventional FSW. An improved grain boundary mobility and dynamic recrystallization cause producing a finer and more refined microstructure in UVaFSWed joints than in traditional FSWed and PVBFSWed joints.

The present study finds better mechanical properties, favorable microstructure, and ductile-type fracture behavior with PVBFSWed and UVaFSWed AA7075-T651 joints compared to the conventional FSWed joint. However, better results are obtained with UVaFSW. Further studies are required to optimize the UVaFSW, considering the effect of different interlayers, process parameters, and tool-pin geometries. Studies are also needed to improve the joint efficiency of UVaFSW of AA7075 alloys considering post-weld treatments.

UVaFSW is mostly attempted for joining Al alloy. Because of its improved mechanical qualities, superior surface quality, and lower defect rate as compared to FSW, UAFSW has drawn interest from several sectors. For welding lightweight aluminum and magnesium alloys, which are frequently used in aerospace components like spacecraft wings and fuselages, UAFSW is quite helpful. Large aluminum fuel tanks and cryogenic storage tanks for space exploration are two possible uses for UAFSW. UAFSW is being investigated for connecting Al alloy battery casings, which call for strong, flawless welds, considering the growing popularity of electric vehicles (EV). The excellent mechanical and surface quality of UAFSW contributes to the extended life and dependability of EV battery packs. To minimize the need for post-processing, UAFSW can assist in the welding of aluminum panels and chassis components with greater mechanical strength and a smoother surface finish. UAFSW is suited for applications where precision welding is necessary to minimize leaks, such as automobile heat exchangers and radiators, because of its ability to weld tiny areas with low flaws. In sectors where lightweight, defect-free, high-strength joints are required, UAFSW provides significant benefits. The industries leading the use of this method for connecting sophisticated alloys with improved mechanical characteristics, superior surface finishes, and reduced defect rates include aerospace, automotive, electronics, military, nuclear, and energy.

Hybridizing natural and synthetic fibers for various applications, such as structural, military, aerospace, and automotive vehicles, is gaining market share due to sustainability and environmental awareness. Polyvinyl Butyral and Kenaf offer eco-friendly solutions, but scientists are exploring natural fiber alternatives. This study found a scope for further studies on the FSW of PVB-layered surfaces considering the effect of ultrasonic vibrations (Salman 2022, Salman 2019, Salman *et al*. 2015). However, further studies are required for joining harder alloys using reliable, wear resistant and economical tools (Auwal *et al*. 2019). Attempts have been made on investigating the fatigue behavior of welded joints with different filler metals (Alioua *et al*. 2017). Studies are also required to comparatively evaluate the fatigue behavior of polyvinyl butyral interlayered and ultrasonic vibration-assisted friction stir welded AA7075-T651 joints.

## 4. Conclusions

This study investigated the performance of polyvinyl butyral interlayered friction stir welded (PVBFSWed) and ultrasonic vibration-assisted friction stir welded (UVaFSWed) AA7075-T651 joints. The joints are produced using the conical threaded pin type tool at different tool rotational and welding speeds. The joints' tensile strength, microhardness, microstructure, and fracture behavior are evaluated. The grain distribution, material flow at the weld nugget, and joint fracture surfaces after the tensile test are investigated with SEM images. The following conclusions could

be drawn from the present work:

• The UVaFSWed joint showed higher tensile strength, microhardness at WN, and minimum surface roughness compared to the PVBFSWed and conventional FSWed joints. The maximum UTS and microhardness at WN of 322.8 MPa and 157 Hv, respectively, for the UVaFSWed joint, were obtained at a tool rotation of 2000 rpm and welding speed of 40 mm/min. However, the lower surface roughness of 7.98 μm was obtained using a tool rotation of 1400 rpm and a welding speed of 40 mm/min.

• The microhardness of the PVBFSWed and UVaFSWed joints showed variation in the welding zones, following the distribution of a letter 'W' shape and found maximum at the WN and minimum at the HAZ. The higher microhardness values were observed in the UVaFSW compared to the PVBFSWed and conventional FSWed joints.

• The appropriate fusion of the material in the WN, the pasty material flow, the joint free of tunnel defect and voids, and a homogeneous distribution of finer grains were observed in the UVaFSWed joint compared to the PVBFSWed and conventional FSWed joints.

• All the test specimens of the PVBFSWed and UVaFSWed joints were fractured in the HAZ due to lower microhardness and showed ductile behavior during fracture. The PVBFSWed joints showed smaller size deep dimples in the microstructure, indicating the lower plastic deformation at the WN. However, larger, equiaxed, and shallow dimples were observed on the fractured surface of the UVaFSWed joints resulting in the higher UTS and microhardness.

• The mechanical properties, microstructure observed in welding zones, and material flow for PVBFSWed joints are superior to the conventional FSWed joints but inferior compared to the UVaFSWed joints. This study finds scope for further work to improve the joint efficiency of UVaFSW of AA7075 alloys using post-weld treatments.

## References

Alioua, A., Bouchouicha, B., Zemri, M. and Abdellatif, I.M.A.D. (2017), "Fatigue behavior of mechanical structures welded with different filler metal", *Adv. Mater. Res*., **6**(3), 233. https://doi.org/10.12989/amr.2017.6.3.233.

Arora, A., De, A. and Debroy, T. (2011), "Toward optimum friction stir welding tool shoulder diameter", *Scr. Mater*., **64**(1), 9-12. https://doi.org/10.1016/j.scriptamat.2010.08.052.

Auwal, S.T., Ramesh, S., Tan, C., Zhang, Z., Zhao, X. and Manladan, S.M. (2019), "Recent developments and challenges in welding of magnesium to titanium alloys", *Adv. Mater. Res*., **8**(1), 47-73. https://doi.org/10.12989/amr.2019.8.1.047.

Boucherit, A., Avettand-Fènoël, M.N. and Taillard, R. (2017), "Effect of a Zn interlayer on dissimilar FSSW of Al and Cu", *Mater. Des*., **124**, 87-99. https://doi.org/10.1016/j.matdes.2017.03.063.

Cetkin, E., Çelik, Y.H. and Temiz, S. (2019), "Microstructure and mechanical properties of AA7075/AA5182 jointed by FSW", *J. Mater. Process. Technol*., **268**, 107-116. https://doi.org/10.1016/j.jmatprotec.2019.01.005.

Chinchanikar, S. and Gaikwad, V.S. (2021), "State of the art in friction stir welding and ultrasonic vibration-assisted friction stir welding of similar/dissimilar aluminum alloys", *J. Comput. Appl. Res. Mech. Eng*., **11**(1), 67-100. https://doi.org/10.22061/JCARME.2021.7390.1983.

Chowdhury, A., Sengupta, K., Maji, K.K., Roy, S. and Ghosal, S. (2021), "Investigation of mechanical properties of dissimilar joint of Al6063 aluminium alloy and C26000 copper alloy by ultrasonic assisted friction stir welding", *Mater. Today Proc.*, **50**, 1527-1534. https://doi.org/10.1016/j.matpr.2021.09.103.

Gaikwad, V.S. and Chinchanikar, S. (2021a), "Mechanical behaviour of friction stir welded AA7075-T651 joints considering the effect of tool geometry and process parameters", *Adv. Mater. Proc Technol*., **8**(4),

3730-3748. https://doi.org/10.1080/2374068X.2021.1976554.
Gaikwad, V.S. and Chinchanikar, S. (2021b), "Investigation on surface roughness, ultimate tensile strength, and microhardness of friction stir welded AA7075-T651 joint", *Mater. Today Proc*., **46**(17), 8061-8065. https://doi.org/10.1016/j.matpr.2021.03.034.
Gaikwad, V.S. and Chinchanikar, S.S. (2022a), "Adaptive neuro fuzzy inference system to predict the mechanical properties of friction stir welded AA7075-T651 joints", *Jordan J. Mech. Ind. Eng*., **16**(3), 381-393.
Gaikwad, V.S. and Chinchanikar, S. (2022b), "Mechanical properties, microstructure, and fracture behavior of friction stir welded AA7075 joints with conical pin and conical threaded pin type tools", *Sci. Iranica*., **30**(1), 1-15. https://doi.org/10.24200/SCI.2022.59154.6087.
Gao, S., Wu, C.S., Padhy, G.K. and Shi, L. (2016), "Evaluation of local strain distribution in ultrasonic enhanced Al 6061-T6 friction stir weld nugget by EBSD analysis", *Mater. Des*., **99**, 135-144. https://doi.org/10.1016/j.matdes.2016.03.055.
Gao, S., Wu, C.S. and Padhy, G.K. (2017), "Material flow, microstructure and mechanical properties of friction stir welded AA 2024-T3 enhanced by ultrasonic vibrations", *J. Manuf. Proc*., **30**, 385-395. https://doi.org/10.1016/j.jmapro.2017.10.008.
Hu, Y., Liu, H. and Du, S. (2021), "Achievement of high-strength 2219 aluminum alloy joint in a broad process window by ultrasonic enhanced friction stir welding", *Mater. Sci. Eng. A*, **804**, 140587. https://doi.org/10.1016/j.msea.2020.140587.
Ji, S., Meng, X., Liu, Z., Huang, R. and Li, Z. (2017), "Dissimilar friction stir welding of 6061 aluminum alloy and AZ31 magnesium alloy assisted with ultrasonic", *Mater. Lett*., **201**, 173-176. https://doi.org/10.1016/j.matlet.2017.05.011.
Khajeh, R., Jafarian, H.R., Jabraeili, R., Eivani, A.R., Seyedein, S. H., Park, N. and Heidarzadeh, A. (2022), "Strength-ductility synergic enhancement in friction stir welded AA2024 alloy and copper joints: Unravelling the role of Zn interlayer's thickness", *J. Mater. Res. Technol*., **16,** 251-262. https://doi.org/10.1016/j.jmrt.2021.11.133.
Kuang, B., Shen, Y., Chen, W., Yao, X., Xu, H., Gao, J. and Zhang, J. (2015), "The dissimilar friction stir lap welding of 1A99 Al to pure Cu using Zn as filler metal with 'pinless' tool configuration", *Mater. Des*., **68**, 54-62. https://doi.org/10.1016/j.matdes.2014.12.008.
Kumar, S. (2016), "Ultrasonic assisted friction stir processing of 6063 aluminum alloy", *Arch. Civ. Mech. Eng.,* **16**(3), 473-484. https://doi.org/10.1016/j.acme.2016.03.002.
Kumar, S., Wu, C.S., Padhy, G.K. and Ding, W. (2017), "Application of ultrasonic vibrations in welding and metal processing: A status review", *J. Manuf. Proc*, **26**, 295-322. https://doi.org/10.1016/j.jmapro.2017.02.027.
Kumar, M., Das, A. and Ballav, R. (2019), "Influence of interlayer on microstructure and mechanical properties of friction stir welded dissimilar joints: A review", *Mater. Today Proc*., **26**, 2123-2129. https://doi.org/10.1016/j.matpr.2020.02.458.
Kumar, S. and Wu, C. (2021), "Eliminating intermetallic compounds via Ni interlayer during friction stir welding of dissimilar Mg/Al alloys", *J. Mater. Res. Technol*., **15**, 4353-4369. https://doi.org/10.1016/j.jmrt.2021.10.065.
Lei, Z., Bi, J., Li, P., Guo, T., Zhao, Y. and Zhang, D. (2018), "Analysis on welding characteristics of ultrasonic assisted laser welding of AZ31B magnesium alloy", *Opt. Laser Technol*., **105**, 15-22. https://doi.org/10.1016/j.optlastec.2018.02.050.
Lenin, W.A., Periyasamy, N. and George, L. (2016), "Influence of interlayer thickness (Zn) on the Properties of Al 7020 FSW Joints", *Mater. Res*., **19**(4), 817-823. https://doi.org/10.1590/1980-5373-MR-2016-0163.
Liu, X.C. and Wu, C.S. (2013), "Experimental study on ultrasonic vibration enhanced friction stir welding", *Proceedings of the 1st International Joint Symposium on Joining and Welding,* 151-154, Osaka, Japan, November. https://doi.org/10.1533/978-1-78242-164-1.151.
Liu, X., Wu, C. and Padhy, G.K. (2015), "Characterization of plastic deformation and material flow in ultrasonic vibration enhanced friction stir welding", *Scr. Mater*., **102**, 95-98. https://doi.org/10.1016/j.scriptamat.2015.02.022.

Liu, X.C. and Wu, C.S. (2015), "Material flow in ultrasonic vibration enhanced friction stir welding", *J. Mater. Sci. Technol*., **225**, 32-44. https://doi.org/10.1016/j.jmatprotec.2015.05.020.

Liu, X.C. and Wu, C.S. (2016), "Elimination of tunnel defect in ultrasonic vibration enhanced friction stir welding", *Mater. Des*. 2016; 90: 350-358. https://doi.org/10.1016/j.matdes.2015.10.131.

Liu, Z., Meng, X., Ji, S., Li, Z. and Wang, L. (2018), "Improving tensile properties of Al/Mg joint by smashing intermetallic compounds via ultrasonic-assisted stationary shoulder friction stir welding", *J. Manuf. Proc*., **31**, 552-559. https://doi.org/10.1016/j.jmapro.2017.12.022.

Liu, H., Zuo, Y., Ji, S., Dong, J. and Zhao, H. (2022), "Friction stir solideliquid spot welding of Cu to Al assisted by Zn interlayer", *J. Mater. Res. Technol*., **18**, 85-95. https://doi.org/10.1016/j.jmrt.2022.02.067.

Lv, X.Q., Wu, C.S. and Padhy, G.K. (2017), "Diminishing intermetallic compound layer in ultrasonic vibration enhanced friction stir welding of aluminum alloy to magnesium alloy", *Mater. Lett*., **203**, 81-84. https://doi.org/10.1016/j.matlet.2017.05.090.

Lv, X., Wu, C.S., Yang, C. and Padhy, G.K. (2018), "Weld microstructure and mechanical properties in ultrasonic enhanced friction stir welding of Al alloy to Mg alloy", *J. Mater. Process. Technol*., **254**, 145-157. https://doi.org/10.1016/j.jmatprotec.2017.11.031.

Meng, X., Jin, Y., Ji, S. and Yan, D. (2018), "Improving friction stir weldability of Al/Mg alloys via ultrasonically diminishing pin adhesion", *J. Mater. Sci. Technol*., **34**(10), 1817-1822. https://doi.org/10.1016/j.jmst.2018.02.022.

Mokabberi, S.R., Movahedi, M. and Kokabi, A.H. (2018), "Effect of interlayers on softening of aluminum friction stir welds", *Mater. Sci. Eng. A*, **727**, 1-10. https://doi.org/10.1016/j.msea.2018.04.093.

Muhammad, N.A. and Wu, C.S. (2019), "Ultrasonic vibration assisted friction stir welding of aluminium alloy and pure copper", *J. Manuf. Proc*., **39**, 114-127. https://doi.org/10.1016/j.jmapro.2019.02.011.

Muhammad, N.A., Wu, C.S. and Su, H. (2021), "Concurrent influences of tool offset and ultrasonic vibration on the joint quality and performance of dissimilar Al/Cu friction stir welds", *J. Mater. Res. Technol*., **14**, 1035-1051. https://doi.org/10.1016/j.jmrt.2021.07.009.

Padhy, G.K., Wu, C.S., Gao, S. and Shi, L. (2016a), "Local microstructure evolution in Al 6061-T6 friction stir weld nugget enhanced by ultrasonic vibration", *Mater. Des*., **92**, 710-723. https://doi.org/10.1016/j.matdes.2015.12.094.

Padhy, G.K., Wu, C.S. and Gao, S. (2016b), "Subgrain formation in ultrasonic enhanced friction stir welding of aluminium alloy", *Mater. Lett*., **183**, 34-39. https://doi.org/10.1016/j.matlet.2016.07.033.

Salman, S.D. (2022), "The influence of kenaf contents and stacking sequence on drop-weight impact properties of hybrid laminated composites reinforced polyvinyl butyral composites", *J. Ind. Text.*, **51**(5), 8645S-8667S. https://doi.org/10.1177/1528083720937388

Salman, S.D. (2020), "Effects of jute fibre content on the mechanical and dynamic mechanical properties of the composites in structural applications", *Def. Technol.*, **16**(6), 1098-1105. https://doi.org/10.1016/j.dt.2019.11.013

Salman, S.D., Leman, Z., Sultan, M.T.H., Ishak, M.R. and Cardona, F. (2015), "Influence of resin system on the energy absorption capability and morphological properties of plain woven kenaf composites", *IOP Conf. Ser. Mater. Sci. Eng.*, **100**(1), 012053. https://doi.org/10.1088/1757-899X/100/1/012053

Sarkari Khorrami, M., Kazeminezhad, M. and Kokabi, A.H. (2014), "The effect of SiC nanoparticles on the friction stir processing of severely deformed aluminum", *Mater. Sci. Eng. A*., **602**, 110-118. https://doi.org/10.1016/j.msea.2014.02.067.

Shakil, M., Tariq, N.H., Ahmad, M., Choudhary, M.A., Akhter, J.I. and Babu, S.S. (2014), "Effect of ultrasonic welding parameters on microstructure and mechanical properties of dissimilar joints", *Mater. Des*., **55**, 263-273. https://doi.org/10.1016/j.matdes.2013.09.074.

Shi, L., Wu, C.S. and Liu, X.C. (2015), "Modeling the effects of ultrasonic vibration on friction stir welding", *J. Mater. Process. Technol.,* **222**, 91-102. https://doi.org/10.1016/j.jmatprotec.2015.03.002.

Shi, L., Wu, C.S., Padhy, G.K. and Gao, S. (2016), "Numerical simulation of ultrasonic field and its acoustoplastic influence on friction stir welding", *Mater. Des*., **104**, 102-115. https://doi.org/10.1016/j.matdes.2016.05.001.

Siddiq, A. and El Sayed, T. (2011), "Acoustic softening in metals during ultrasonic assisted deformation via CP-FEM", *Mater. Lett.,* **65**(2), 356-359. https://doi.org/10.1016/j.matlet.2010.10.031.

Su, H., Zhao, Q., Chen, J. and Wu, C. (2022), "Homogenizing the intermetallic compounds distribution in Al/Cu dissimilar friction stir welding joint with the assistance of ultrasonic vibration", *Mater. Today Commun*., **31**, 103643. https://doi.org/10.1016/j.mtcomm.2022.103643.

Thomä, M., Wagner, G., Straß, B., Wolter, B., Benfer, S. and Fürbeth, W. (2018), "Ultrasound enhanced friction stir welding of aluminum and steel: Process and properties of EN AW 6061/DC04-Joints," *J. Mater. Sci. Technol*., **34**(1), 163-172. https://doi.org/10.1016/j.jmst.2017.10.022.

Wu, M., Wu, C.S. and Gao, S. (2017), "Effect of ultrasonic vibration on fatigue performance of AA 2024-T3 friction stir weld joints", *J. Manuf. Process*., **29**, 85-95. https://doi.org/10.1016/j.jmapro.2017.07.023.

Wu, C.S., Wang, T. and Su, H. (2022), "Material flow velocity, strain and strain rate in ultrasonic vibration enhanced friction stir welding of dissimilar Al/Mg alloys", *J. Manuf. Process*., **75**, 13-22. https://doi.org/10.1016/j.jmapro.2021.12.055.

Xu, C., Sheng, G., Cao, X. and Yuan, X. (2016), "Evolution of Microstructure, Mechanical Properties and Corrosion Resistance of Ultrasonic Assisted Welded-Brazed Mg/Ti Joint", *J. Mater. Sci. Technol*., **32**(12), 1253-1259. https://doi.org/10.1016/j.jmst.2016.08.029.

Yang, C., Wu, C.S. and Shi, L. (2020), "Effect of ultrasonic vibration on dynamic recrystallization in friction stir welding", *J. Manuf. Proc*., **56**, 87-95. https://doi.org/10.1016/j.jmapro.2020.04.064.

Yao, Z., Kim, G.Y., Faidley, L., Zou, Q., Mei, D. and Chen, Z. (2012), "Effects of superimposed high-frequency vibration on deformation of aluminum in micro/meso-scale upsetting", *J. Mater. Proc. Technol.,* **212**(3), 640-646. https://doi.org/10.1016/j.jmatprotec.2011.10.017.

Zhang, Z., He, C., Li, Y., Yu, L., Zhao, S. and Zhao, X. (2020), "Effects of ultrasonic assisted friction stir welding on flow behavior, microstructure and mechanical properties of 7N01-T4 aluminum alloy joints", *J. Mater. Sci. Technol*., **43**, 1-13. https://doi.org/10.1016/j.jmst.2019.12.007.

Zhao, W., Wu, C.S. and Su, H. (2020), "Numerical investigation of heat generation and plastic deformation in ultrasonic assisted friction stir welding", *J. Manuf. Proc*., **56**, 967-980. https://doi.org/10.1016/j.jmapro.2020.05.047.

Zhao, J., Wu, C.S. and Shi, L. (2022), "Effect of ultrasonic field on microstructure evolution in friction stir welding of dissimilar Al/Mg alloys", *J. Mater. Res. Technol*., **17**, 1-21. https://doi.org/10.1016/j.jmrt.2021.12.133.

Zhong, Y.B., Wu, C.S. and Padhy, G.K. (2017), "Effect of ultrasonic vibration on welding load, temperature and material flow in friction stir welding", *J. Mater. Proc. Technol*., **239**, 273-283. https://doi.org/10.1016/j.jmatprotec.2016.08.025.

*CC*